New Basis Functions for the Electromagnetic Solution of Arbitrarily-shaped, Three Dimensional Conducting Bodies Using Method of Moments

Anne I. Mackenzie[1], Michael E. Baginski[2], Sadasiva M. Rao[3]

[1]NASA Langley Research Center, Hampton, VA 23681 (USA), email:anne.mackenzie-1@nasa.gov
[2]Department of E & CE, Auburn University, Auburn, AL 36849 (USA), email:baginme@auburn.edu
[3]Department of E & CE, Auburn University, Auburn, AL 36849 (USA), email:rao@eng.auburn.edu

Abstract

In this work, we present a new set of basis functions, defined over a pair of planar triangular patches, for the solution of electromagnetic scattering and radiation problems associated with arbitrarily-shaped surfaces using the method of moments solution procedure. The basis functions are constant over the function subdomain and resemble pulse functions for one and two dimensional problems. Further, another set of basis functions, point-wise orthogonal to the first set, is also defined over the same function space. The primary objective of developing these basis functions is to utilize them for the electromagnetic solution involving conducting, dielectric, and composite bodies. However, in the present work, only the conducting body solution is presented and compared with other data.

1 Introduction

The solution of electromagnetic scattering/radiation problems involving arbitrary shapes and material composition is of much interest to commercial as well as defense industries. The method of moments (MoM) [1] solutions to these problems generally involve triangular patch modeling and utilizing Rao-Wilton-Glisson (RWG) basis functions [2]. It may be noted that the RWG basis functions have been primarily defined for the solution of conducting bodies and the utilization of the same basis functions for dielectric/composite bodies is less than satisfactory. The primary difficulty associated with a material body solution is the requirement of two orthogonal basis functions to express unknown electric and magnetic currents $\boldsymbol{J}$ and $\boldsymbol{M}$. In our opinion, using the same basis functions for both $\boldsymbol{J}$ and $\boldsymbol{M}$ is not a good idea and invariably results in numerical difficulties. However, a host of techniques have been developed which involve either tinkering with the basis functions or modifying the testing procedures to apply to material bodies [3, 4, 5]. Keeping these difficulties in perspective, in this work, we present two sets of basis functions, each one point-wise orthogonal to the other function, which can be used for conducting as well as material bodies. The present work, however, involves only conducting bodies along with several numerical results. The solution of the material body problem will be presented in a future article.

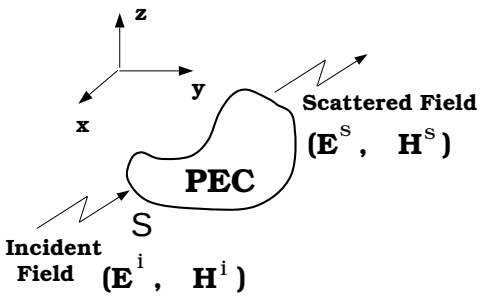

Figure 1: Arbitrarily-shaped conducting body excited by an incident electromagnetic plane wave.

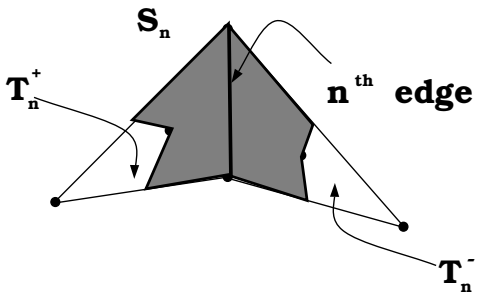

Figure 2: Basis function description.

2 Description of the Problem

Let S denote the surface of an arbitrarily-shaped perfectly conducting body illuminated by an incident electromagnetic plane wave $\boldsymbol{E}^i$ as shown in Figure 1. Using the equivalence principle, potential theory and the free-space Green's function [1], the electric field integral equation (EFIE) is given by

$$[j\omega \boldsymbol{A} + \nabla \Phi]_{tan} \;=\; \boldsymbol{E}^i_{tan} \tag{1}$$

where the subscript "tan" refers to the tangential component. In (1),

$$\boldsymbol{A} \;=\; \mu \int_S \boldsymbol{J}_s \, G \, ds' \tag{2}$$

$$\Phi \;=\; \epsilon^{-1} \int_S q_s \, G \, ds' \tag{3}$$

$$G \;=\; \frac{e^{-jkR}}{4\pi R} \tag{4}$$

$$R \;=\; |\boldsymbol{r} - \boldsymbol{r}'| \tag{5}$$

ϵ and μ are permittivity and permeability of the surrounding medium, k is the wave number and $\boldsymbol{r}$ and $\boldsymbol{r}'$ represent the position vectors to observation and source points, respectively, from a global coordinate origin. The unknown surface current $\boldsymbol{J}_s$ is related to the charge density q_s by the continuity equation, given by

$$\nabla \bullet \boldsymbol{J}_s \;=\; -j\omega \, q_s \tag{6}$$

For the numerical solution of (1), we apply the method of moments formulation using planar triangular patch modeling and the basis functions as described in the following section:

3 Description of Basis Functions

Let T_n^+ and T_n^- represent two triangles connected to the edge n of the triangulated surface model as shown in Figure 2. We define two mutually orthogonal vector basis functions associated with the n^{th} edge as

$$\boldsymbol{f}_n(\boldsymbol{r}) = \begin{cases} \boldsymbol{a}_n^{\pm} \times \hat{\boldsymbol{\ell}}, & \boldsymbol{r} \in S_n, \\ 0, & \text{otherwise} \end{cases} \tag{7}$$

and

$$\boldsymbol{g}_n(\boldsymbol{r}) = \begin{cases} \hat{\boldsymbol{\ell}}, & \boldsymbol{r} \in S_n, \\ 0, & \text{otherwise} \end{cases} \tag{8}$$

where S_n represents the region obtained by connecting the mid-points of the free edges to the centroids of triangles $T_n^{\pm}$, and to the nodes of edge n. Note that this area is shown shaded in the Figure 2. Also, $\hat{\boldsymbol{\ell}}$ and $\boldsymbol{a}_n^{\pm}$ represent the unit vector along the n^{th} edge and the unit normal vector to the plane of the triangle $T_n^{\pm}$, respectively. Note that the basis functions defined in (8) are actually the pulse functions defined over the region S_n. It is well-known that the pulse functions do not have continuous derivatives but result in delta distributions along the boundary. This point is crucial in modeling the charge density and the calculation of scalar potential which may be accomplished as described in the following section. Also, note that in this work, only perfect electric conductor (PEC) bodies are analyzed and hence only $\boldsymbol{f}_n$'s are used in the method of moments solution.

4 Numerical Solution Procedure

As a first step, we consider the testing procedure. Consider the m^{th} interior edge, associated with triangles $T_m^{\pm}$. We integrate the vector component of (1) parallel to the path from the centroid $\boldsymbol{r}_m^{c+}$ of T_m^+, to the midpoint of the edge $\boldsymbol{r}_m$ and thence from $\boldsymbol{r}_m$ to the centroid of T_m^- given by $\boldsymbol{r}_m^{c-}$. For both path integrations, approximate $\boldsymbol{A}$ and $\boldsymbol{E}^i$ by their respective values at the mid-points of each path. Thus, we have,

$$\begin{aligned} j\omega \boldsymbol{A}\left(\frac{\boldsymbol{r}_m + \boldsymbol{r}_m^{c+}}{2}\right) \bullet (\boldsymbol{r}_m - \boldsymbol{r}_m^{c+}) + j\omega \boldsymbol{A}\left(\frac{\boldsymbol{r}_m + \boldsymbol{r}_m^{c-}}{2}\right) \bullet (\boldsymbol{r}_m^{c-} - \boldsymbol{r}_m) + \\ \left[\Phi(\boldsymbol{r}_m^{c-}) - \Phi(\boldsymbol{r}_m^{c+})\right] = \boldsymbol{E}^i\left(\frac{\boldsymbol{r}_m + \boldsymbol{r}_m^{c+}}{2}\right) \bullet (\boldsymbol{r}_m - \boldsymbol{r}_m^{c+}) + \\ \boldsymbol{E}^i\left(\frac{\boldsymbol{r}_m + \boldsymbol{r}_m^{c-}}{2}\right) \bullet (\boldsymbol{r}_m^{c-} - \boldsymbol{r}_m) \end{aligned} \tag{9}$$

for $m = 1, 2, \cdot, N$, where N represents the total number of interior edges in the triangulation scheme, *i.e.* excluding the edges on the boundary for an open body.

Next, we consider the expansion procedure. Using the basis functions $\boldsymbol{f}_n$ defined in (8), we approximate the unknown current $\boldsymbol{J}$ as

$$\boldsymbol{J} = \sum_{n=1}^{N} I_n \boldsymbol{f}_n \tag{10}$$

Next, substituting the current expansion (10) into (9) yields an $N \times N$ system of linear equations which may be written in matrix form as $\boldsymbol{ZI} = \boldsymbol{V}$, where $\boldsymbol{Z} = [Z_{mn}]$ is an $N \times N$ matrix and $\boldsymbol{I} = [I_n]$ and $\boldsymbol{V} = [V_m]$ are column vectors of length N. The elements of the $\boldsymbol{Z}$ and $\boldsymbol{V}$ are given by

$$Z_{mn} = j\omega \left[\boldsymbol{A}_{mn}^{+} \bullet (\boldsymbol{r}_m - \boldsymbol{r}_m^{c+}) + \boldsymbol{A}_{mn}^{-} \bullet (\boldsymbol{r}_m^{c-} - \boldsymbol{r}_m) \right] + \Phi_{mn}^{-} - \Phi_{mn}^{+} \tag{11}$$

$$V_m = \boldsymbol{E}_m^{+} \bullet (\boldsymbol{r}_m - \boldsymbol{r}_m^{c+}) + \boldsymbol{E}_m^{-} \bullet (\boldsymbol{r}_m^{c-} - \boldsymbol{r}_m) \tag{12}$$

where

$$\boldsymbol{A}_{mn}^{\pm} = \mu \int_S \boldsymbol{f}_n \frac{e^{-jkR_m^{\pm}}}{4\pi R_m^{\pm}} \, dS' \tag{13}$$

$$\Phi_{mn}^{\pm} = \frac{-1}{j\omega\epsilon} \int_S \nabla_s \bullet \boldsymbol{f}_n \frac{e^{-jkR_m^{c\pm}}}{4\pi R_m^{c\pm}} \, dS' \tag{14}$$

$$R_m^{\pm} = \left| \frac{\boldsymbol{r}_m + \boldsymbol{r}_m^{c\pm}}{2} - \boldsymbol{r}' \right| \tag{15}$$

$$R_m^{c\pm} = |\boldsymbol{r}_m^{c\pm} - \boldsymbol{r}'| \tag{16}$$

$$\boldsymbol{E}_m^{\pm} = \boldsymbol{E}^i \left(\frac{\boldsymbol{r}_m + \boldsymbol{r}_m^{c\pm}}{2} \right) \tag{17}$$

The numerical evaluation of the vector potential, shown in (13), is straightforward and may be accomplished by the procedure described in [6]. However, the numerical evaluation of the scalar potential term, described in (14), may be carried out as follows:

Let us define the unknown charge density q_s in (3), as

$$q_s = \sum_{i=1}^{N_p} \alpha_i P_i \tag{18}$$

where N_P represents the number of triangular patches in the model, α_i is the unknown coefficient, and

$$P_i(\boldsymbol{r}) = \begin{cases} 1, & \boldsymbol{r} \in T_i \\ 0, & \text{otherwise} \end{cases} \tag{19}$$

Next, consider a triangular patch T_i with associated non-boundary edges, i_1, i_2, and i_3. Then, using (6), the well-known Divergence theorem, and simple vector calculus, we have

$$\begin{aligned} \int_{T_i} q_s ds &= \int_{T_i} \frac{\nabla_s \bullet \boldsymbol{J}}{-j\omega} \, ds \\ &= \frac{j}{\omega} \oint_{C_i} \boldsymbol{J} \bullet \boldsymbol{n}_\ell \boldsymbol{dl} \\ &= \frac{j}{\omega} [I_{i_1} \ell_{i_1} + I_{i_2} \ell_{i_2} + I_{i_3} \ell_{i_3}] \end{aligned} \tag{20}$$

where C_i is the contour bounding the triangle T_i, $\boldsymbol{n}_\ell$ is the unit normal vector to the contour C_i in the plane of T_i, and $\ell_{i_j}, j = 1, 2, 3$ represent the edge lengths. Also, note that

$$\begin{aligned} \int_{T_i} q_s ds &= \int_{T_i} \alpha_i ds \\ &= \alpha_i A_i \end{aligned} \tag{21}$$

where A_i represents the area of the triangle T_i. Lastly, using (20) and (21), we have

$$\alpha_i = \frac{j}{\omega}\left[\frac{I_{i_1}\ell_{i_1} + I_{i_2}\ell_{i_2} + I_{i_3}\ell_{i_3}}{A_i}\right] \tag{22}$$

Thus, we can write the scalar potential term in (14) as,

$$\Phi_{mn}^{\pm} = \frac{j\ell_n}{\omega\epsilon}\left[\frac{1}{A_{n^+}}\int_{T_n^+}\frac{e^{-jkR_m^{c\pm}}}{4\pi R_m^{c\pm}}\,dS' - \frac{1}{A_{n^-}}\int_{T_n^-}\frac{e^{-jkR_m^{c\pm}}}{4\pi R_m^{c\pm}}\,dS'\right] \tag{23}$$

Finally, once the matrices $\boldsymbol{Z}$ and $\boldsymbol{V}$ are determined, one may easily solve the system of linear equations to obtain $\boldsymbol{I}$.

5 Numerical Results

In this section, we present numerical results for a square plate (length = 0.15λ), circular disk (diameter = 0.15λ), a sphere (diameter = 0.15λ) and a circular cylinder (diameter = 0.15λ, length = 0.15λ), and compare with the solution obtained using the procedure presented in [2]. Also, for the case of the sphere, the results are compared with the exact solution. The plate, the disk, the sphere, and the cylinder are modeled with 312, 258, 500, and 320 triangles, respectively. In every case, the body is placed at the center of the coordinate system and illuminated by an x-polarized plane wave traveling along the z-axis. Further, the square plate and the circular disk are oriented parallel to the xy-plane. The bistatic radar cross section (RCS) is presented in figures 3, 4, 5, and 6. We note that the results compare well with the other numerical results.

6 Conclusions

In this work, we present a new set of basis functions for the method of moments solution of electromagnetic scattering by conducting bodies of arbitrary shape. The new basis functions are pulse basis functions defined over a pair of triangular patches. Another set of basis functions, point-wise orthogonal to the first set, is also presented. It is hoped that these two sets of basis functions, in conjunction with the method of moments solution procedure, provide a more stable solution to material problems. However, in the present work, only conducting scatterers are analyzed with the new basis functions and the results are compared with those from other solution methods. At present, the work is in progress to apply the new basis functions to material bodies and will be reported in the future.

References

[1] R. F. Harrington, *Time-Harmonic Electromagnetic Fields*, New York, McGraw-Hill, 1961.

[2] S. M. Rao, D. R. Wilton, and A. W. Glisson, "Electromagnetic Scattering by Surfaces of Arbitrary Shape", *IEEE Transactions on Antennas and Propagation,* Vol. 30, pp. 409 - 418, 1982.

[3] S. M. Rao and D. R. Wilton, "E-field, H-field, and Combined Field Solution for Arbitrary Shaped Three Dimensional Dielectric Objects", *Electromagnetics*, vol. 10, pp. 407 - 421, October - December 1990.

[4] S. M. Rao, T. K. Sarkar, P. Midya, and A. R. Djordjevic, "Electromagnetic Scattering from Finite Conducting and Dielectric Structures : Surface/Surface Formulation", *IEEE Transactions Antennas and Propagation*, vol. 39, pp. 1034 - 1037, July 1991.

[5] X. Q. Sheng, J. M. Jin, J. Song, W. C. Chew, C. C. Lu, "Solution of combined-field integral equation using multilevel fast multipole algorithm for scattering by homogeneous bodies", *IEEE Transactions Antennas and Propagation*, vol. 46, pp. 1718 - 1726, November 1998.

[6] D. R. Wilton, S. M. Rao, A. W. Glisson, D. H. Schaubert, O. M. Al-Bundak, and C. M. Butler, "Potential Integrals for Uniform and Linear Source Distributions on Polygonal and Polyhedral Domains ", *IEEE Transactions on Antennas and Propagation*, vol. 32, pp. 276 - 281, March 1984.

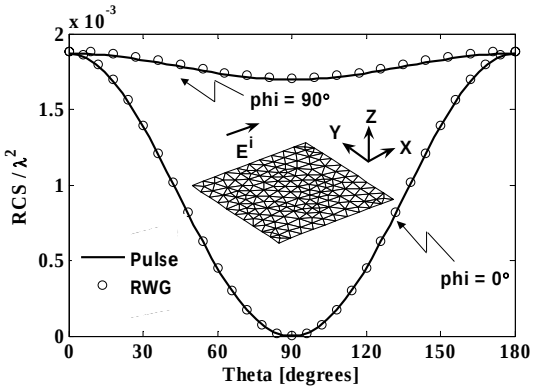

Figure 3: Bistatic RCS of a square plate.

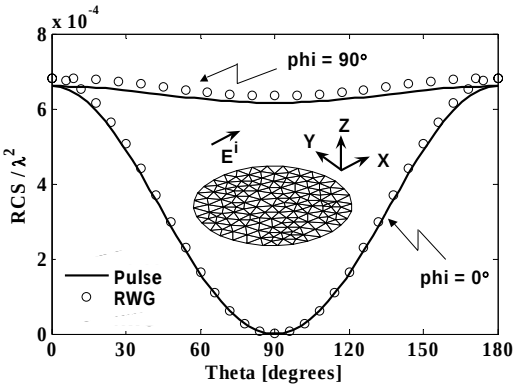

Figure 4: Bistatic RCS of a circular disk.

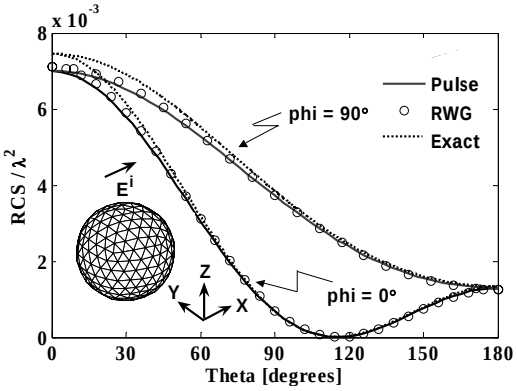

Figure 5: Bistatic RCS of a sphere.

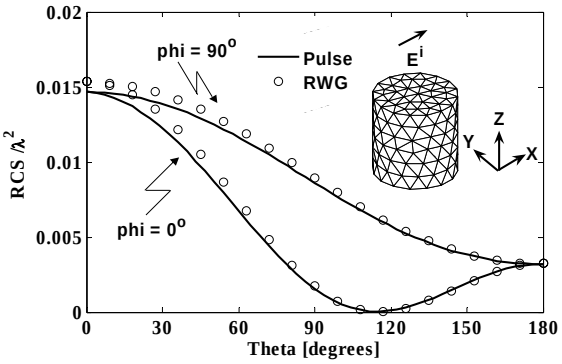

Figure 6: Bistatic RCS of a circular cylinder.